ACS APPLIED MATERIALS & INTERFACES

Research Article

www.acsami.org

Monodisperse Mesoporous Carbon Nanoparticles from Polymer/Silica Self-Aggregates and Their Electrocatalytic Activities

Xiaoxi Huang,[†] Li-Jing Zhou,[∥] Damien Voiry,[§] Manish Chhowalla,[§] Xiaoxin Zou,*[,∥] and Tewodros Asefa*[,†,‡]

[†]Department of Chemistry and Chemical Biology, Rutgers, [‡]Department of Chemical and Biochemical Engineering, Rutgers, and [§]Department of Materials Science and Engineering, Rutgers, The State University of New Jersey, Piscataway, New Jersey 08854, United States

[∥]State Key Laboratory of Inorganic Synthesis and Preparative Chemistry, International Joint Research Laboratory of Nano-Micro Architecture Chemistry, College of Chemistry, Jilin University, Changchun 130012, China

Supporting Information

ABSTRACT: In our quest to make various chemical processes sustainable, the development of facile synthetic routes and inexpensive catalysts can play a central role. Herein we report the synthesis of monodisperse, polyaniline (PANI)-derived mesoporous carbon nanoparticles (PAMCs) that can serve as efficient metal-free electrocatalysts for the hydrogen peroxide reduction reaction (HPRR) as well as the oxygen reduction reaction (ORR) in fuel cells. The materials are synthesized by polymerization of aniline with the aid of $(NH_4)_2S_2O_8$ as oxidant and colloidal silica nanoparticles as templates, then carbonization of the resulting PANI/silica composite material at different high temperatures, and finally removal of the silica templates from the carbonized products. The PAMC materials that are synthesized under optimized synthetic conditions possess monodisperse mesoporous carbon nanoparticles with an average size of 128 ± 12 nm and an average pore size of ca. 12 nm. Compared with Co_3O_4, a commonly used electrocatalyst for HPRR, these materials show much better catalytic activity for this reaction. In addition, unlike Co_3O_4, the PAMCs remain relatively stable during the reaction, under both basic and acidic conditions. The nanoparticles also show good electrocatalytic activity toward ORR. Based on the experimental results, PAMCs' excellent electrocatalytic activity is attributed partly to their heteroatom dopants and/or intrinsic defect sites created by vacancies in their structures and partly to their high porosity and surface area. The reported synthetic method is equally applicable to other polymeric precursors (e.g., polypyrrole (PPY)), which also produces monodisperse, mesoporous carbon nanoparticles in the same way. The resulting materials are potentially useful not only for electrocatalysis of HPRR and ORR in fuel cells but also for other applications where high surface area, small sized, nanostructured carbon materials are generally useful for (e.g., adsorption, supercapacitors, etc.).

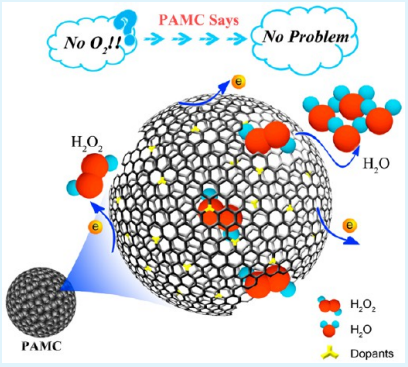

KEYWORDS: *mesoporous carbon, carbon nanomaterial, metal-free catalyst, hydrogen peroxide reduction, polyaniline*

INTRODUCTION

The development of size- and morphology-controlled, advanced functional nanomaterials still remains one of the most important goals in nanomaterials research. This includes the synthesis of porous carbon nanomaterials, which have a diverse range of applications in areas including drug delivery, renewable energy, separations, nanoelectronics, and catalysis.[1−3] Developing these materials with spherical morphology with diameters of less than 200 nm, in particular, is of huge interest due to the added advantages such materials have for the aforementioned applications, especially for those that rely on good mass transport within the materials' structures.[4] For example, smaller carbon nanospheres are shown to have better pseudocapacitance than their bigger counterparts because their small, nanoscale size shortens the transport pathways for ions, making ion diffusion and mass transport through the structures of these materials easier.[5]

In order to make spherical carbon nanoparticles/microparticles, several approaches including hard templating,[6−14] soft templating,[4,15−19] and various extensions of the Stöber synthetic method[20−23] have been developed. In many of these cases, the precursors that were mainly used to make the materials include carbohydrates (glucose,[7,8] sucrose,[13] cyclodextrins[17]), phenolic resins (phenol−formaldehyde,[8,16,22] resorcinol−formaldehyde[12,15,18,20,23]), furfuryl alcohol,[6] dopamine,[4,10,14] etc. But polymers, such as polyaniline (PANI) and polypyrrole (PPY), are more appealing precursors for making heteroatom-doped carbon materials because they have a high nitrogen (heteroatom) content, are easily "carbonizable", and are easier to synthesize in solutions.[24−26] Moreover, PANI

Received: May 13, 2016
Accepted: June 30, 2016
Published: June 30, 2016

DOI: 10.1021/acsami.6b05739
ACS Appl. Mater. Interfaces 2016, 8, 18891−18903

or PPY can form some spherical aggregates with colloidal silica,[27−29] and by using the resulting PANI/silica or PPY/silica aggregates as precursor, spherical mesoporous carbon nanoparticles can be synthesized.[30]

Recently, the potential application of carbon nanomaterials for electrocatalysis of various reactions that are pertinent to renewable energy systems has become a major focus of research for these materials. This is mainly the result of a number of unprecedented findings over the past few years revealing that even if they do not contain metals, some carbon materials can still catalyze different important reactions that are commonly employed in various fuel cells and electrolyzers. For example, heteroatom-doped carbon nanomaterials have been shown to catalyze the oxygen reduction reaction (ORR).[31−39] This reaction, which involves oxygen as oxidant, is critically important to the performance of a variety of fuel cells. However, although ORR is vital in many types of fuel cells, in some environments (e.g., the outer space or under the sea) where there is no air or the amount of oxygen is very limited, and plus the transportation of oxygen gas to these locations is quite difficult or costly, it is difficult, if not impossible, to apply ORR in fuel cells. In such environments, hydrogen peroxide can be a more suitable oxidant for the fuel cells, since it can oxidize fuels (as much as oxygen does), is easily portable (as it is liquid under most conditions), has a high power density, and possesses low activation energy with fast reduction kinetics. Hence, finding sustainable catalysts for the hydrogen peroxide reduction reaction (HPRR) for use in hydrogen peroxide oxidant-based fuel cells is appealing.[40,41]

While metal-free electrocatalysts that have the potential to replace noble metal catalysts such as Pt have slowly been making to the stage,[31−39] most of the catalysts for HPRR are still based on metals or metal oxides, such as palladium, copper, cobalt oxide, or gold.[41−48] Moreover, as many types of fuel cells are generally operated under acidic or basic environments, the long-term stability of many of these metallic and metal oxide catalysts, which can easily leach, corrode, and/or dissolve under the HPRR conditions, remains a major issue. These properties of metals or metal oxides also make these catalysts not good candidates for reduction of H_2O_2 that can be directly generated from oxygen via ORR in acidic solution using solar energy.[49] Hence, exploring the potential of carbon-based catalysts, which are sustainable and stable under many reaction conditions, for HPRR electrocatalysis deserves a special attention.

It is also worth adding that the ORR can proceed via either a 4-electron or a [2 + 2]-electron pathway. When ORR proceeds through a [2 + 2]-electron process, the process gives peroxide or superoxide intermediates and can thus involve HPRR in the second, 2-electron step.[50−52] While some materials are reported to catalyze both ORR and HPRR independently, based on previous studies with metallic-based catalysts (e.g., cobalt oxide and Pd), the catalysts can exhibit notable differences in the two reactions.[45,46,53,54] This is not surprising, given the fact that ORR and HPRR, as well as the conditions under which the two reactions take place, are not necessarily the same (even if HPRR can be considered as a subset of the [2 + 2]-electron ORR). For example, unlike the relatively high concentration of H_2O_2 present in HPRR, the concentration of H_2O_2 in a 4-electron ORR can be quite small because the H_2O_2 that forms as intermediate during the reaction gets consumed as soon as it is formed. There is also an inherent competition between O_2 and H_2O_2 for the available catalytic sites over the catalyst's surface during a [2 + 2]-electron ORR; however, this is largely not the case in HPRR, unless it goes through H_2O_2 decomposition.

Notably also, despite several reports on carbon-based materials for ORR electrocatalysis, there has been limited study on these materials for HPRR electrocatalysis. Moreover, the fact that some carbon-based catalysts have been reported to form H_2O_2 as selective product during ORR[55,56] suggests that these materials are ineffective as catalyst for HPRR (or for the second possible process in the [2 + 2]-electron ORR).

Herein we report a facile synthetic route that can produce nanosized (128 ± 12 nm) polyaniline-derived mesoporous carbon nanospheres (denoted as PAMCs) that show efficient electrocatalytic activities toward HPRR as well as ORR, in both acidic and basic conditions. These metal-free electrocatalytically active materials have high porosity, high surface area, and large density of heteroatom dopants and/or defect sites created by vacancies on their carbon structures. They are synthesized by using PANI as a precursor and silica nanoparticles as templates. Similar materials are also shown to form using PPY as a precursor. The synthetic conditions that can lead to PAMC materials with high electrocatalytic activity for HPRR and some of the structural factors that influence their electrocatalytic activity toward HPRR are also discussed.

EXPERIMENTAL SECTION

Materials. Colloidal silica dispersion (Ludox HS-40, 40 wt % suspension in water), aniline, ammonium persulfate, potassium hydroxide, sulfuric acid, hydrochloric acid, hydrogen peroxide solution (30 wt % in H_2O), platinum on graphitized carbon (20 wt % loading), Nafion perfluorinated resin solution, and 2-propanol were all obtained from Sigma-Aldrich. Sodium hydroxide was purchased from Fisher Scientific. All the reagents were of analytical grade and used as received without further purification. Distilled water was used throughout the experiments.

Synthesis of Polyaniline−Silica (PANI-SiO_2) Nanocomposite Materials and PANI. Different amounts of reagents and procedures, as described in detail in Table S1, were used for the synthesis of different polyaniline (PANI)−silica nanocomposite (PANI-SiO_2) materials. Typically, as-synthesized PANI-SiO_2 was synthesized through polymerization of aniline in the presence of ammonium persulfate (oxidant) and colloidal silica templates. First, 15 g (11.5 mL) of colloidal silica, 1 mL (10.5 mmol) of aniline, and 1 M aqueous HCl solution (60 mL) were mixed. The solution was stirred at a temperature between 0 and 5 °C for 10 min. Then, into this solution, 1 M aqueous HCl solution (12 mL) containing ammonium persulfate (2.5 g, 11.0 mmol) was added. The solution was then stirred for 4 h at a temperature between 0 and 5 °C. The solution was finally kept at 100 °C to let the solvent evaporate. The resulting dried, solid product was named PANI−SiO_2.

Additionally, three more materials were synthesized, namely (1) PANI-SiO_2-H_2O, which is a PANI−silica nanocomposite material prepared by following the same procedures as the one above, except by using pure water instead of 1 M aqueous HCl solution, (2) PANI-SiO_2-15, which is a PANI−silica nanocomposite material synthesized using less amount (15 mL) of 1 M aqueous HCl solution (note that 60 mL of 1 M aqueous HCl solution was used for making PANI-SiO_2), and (3) PANI (without silica) was synthesized by polymerization of aniline in the absence of colloidal silica templates, with otherwise similar synthetic procedure as above.

Preparation of Various Mesoporous Carbon (Nano)-materials by Thermal Treatment of the PANI-SiO_2 Precursors and PANI. The different PANI-SiO_2 nanocomposite materials synthesized above were carbonized at high temperatures. In a typical experiment, 1 g of PANI-SiO_2 was placed in an alumina boat within a tube furnace and heated under an inert atmosphere (argon) from 25 to 300 °C at a ramp of 1 °C/min. After keeping the sample at 300 °C for 3 h, the temperature was raised to a final pyrolysis temperature of 700,

DOI: 10.1021/acsami.6b05739
ACS Appl. Mater. Interfaces 2016, 8, 18891−18903

Scheme 1. Synthetic Procedure Employed To Make Polyaniline (PANI)-Derived Mesoporous Carbon Nanoparticles (PAMCs): (1) Synthesis of a PANI/Colloidal Silica Nanocomposite Material, (2) Pyrolysis of the Composite Material at Different High Temperatures, and (3) Etching of the Silica Nanoparticles from the Carbonized Product with Aqueous NaOH Solution

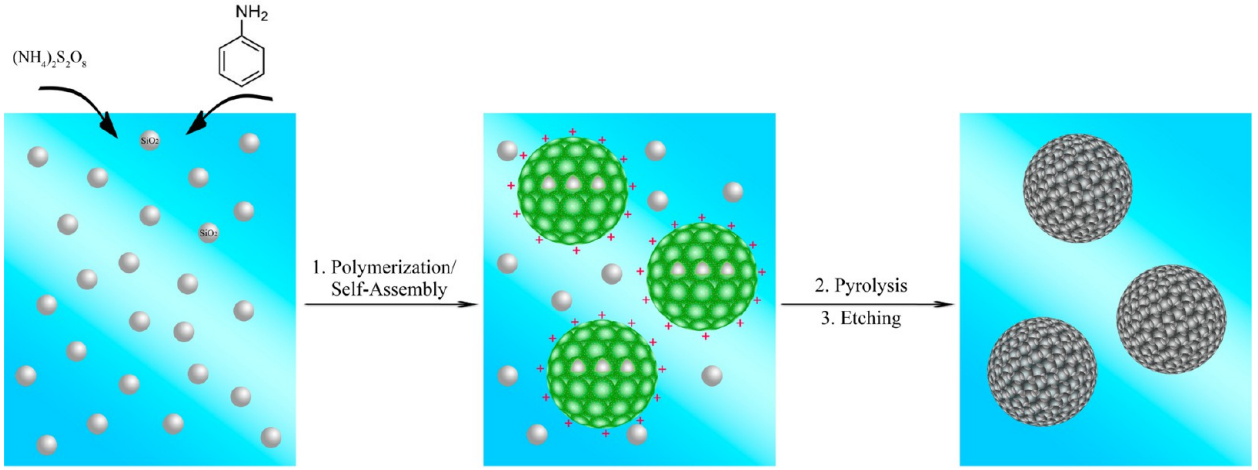

800, 900, or 1000 °C with a ramp of 10 °C/min. The materials were kept at this temperature for 2 h and then let to cool down to room temperature. Subsequently, the silica in the pyrolyzed materials was etched by mixing 270 mg of the sample with 18 mL of aqueous NaOH solution (2 M) and keeping the resulting mixtures in an autoclave at 100 °C for 18 h. Finally, the mixtures were centrifuged, and the solid products were recovered and washed with distilled water until their supernatants became neutral. The materials were let to dry under ambient conditions. The resulting PANI-derived mesoporous nanoparticles were denoted as PAMC-*T*, where *T* represents their final pyrolysis temperatures: 700, 800, 900, or 1000 °C (i.e., PAMC-700, PAMC-800 PAMC-900, and PAMC-1000, respectively).

Similarly, the PANI-SiO_2-H_2O, PANI-SiO_2-15, and PANI synthesized above were carbonized by heating each material at the final pyrolysis temperature of 900 °C. After treating the resulting carbonized products with NaOH solution as above, different types of carbon materials, denoted as PAMC-900-H_2O, PAMC-900-15, and PANC-900, respectively, were obtained. Comparative details of the reagents and synthetic conditions used to make all the above carbon materials are compiled in Table S1.

Synthesis of Poly(fufuryl alcohol)-Derived Mesoporous Carbon. Poly(fufuryl alcohol)−SiO_2 composite material was prepared by polymerization of fufuryl alcohol in 1 M aqueous HCl solution in the presence of colloidal silica templates. Typically, 7.5 g (5.75 mL) of colloidal silica and 1 M aqueous HCl solution (30 mL) were mixed. The solution was stirred at room temperature for 10 min before adding fufuryl alcohol (0.5 mL) in it. The solution was then stirred for 24 h at room temperature. The solution was finally kept at 100 °C to let the solvent evaporate.

Like the procedure used to make PAMC-900, the resulting dried solid product was pyrolyzed with a similar heating sequence as above, using a final temperature of 900 °C. The carbonized product was finally treated with NaOH solution to remove the silica material in it, in the same way as above. After washing the product with water and letting it dry under ambient conditions, poly(fufuryl alcohol)-derived mesoporous carbon material (named as FAMC-900) was obtained.

Synthesis of Polypyrrole-Derived Mesoporous Carbon. In a typical synthesis of this material, 1 mL of pyrrole, 15 g (11.5 mL) of silica nanoparticles, and 1 M HCl (60 mL) were mixed. The solution was stirred at a temperature between 0 and 5 °C for 10 min. Then, into the solution, 1 M HCl (12 mL) containing ammonium persulfate (3.5 g, 15.3 mmol) was added. The reaction mixture was stirred for an additional 5 h on ice bath, and the solvent in the mixture was then evaporated. The solid material was pyrolyzed at 900 °C, and the silica nanoparticle templates were removed from the carbonized product with aqueous NaOH solution in the same way as above. After washing the product with water and letting it dry under ambient conditions, PPY-derived mesoporous carbon nanoparticles were obtained.

Preparation of Electrodes for Electrochemical Measurement. The eletrocatalytic properties of the carbon materials toward HPRR were evaluated with a PAR (Princeton Applied Research) Versastat3 potentiostat using a three-electrode system. The cell consisted of a saturated calomel electrode (SCE) as a reference electrode, a carbon rod (diameter: 6 mm) as a counter electrode, and a glassy carbon disk (diameter: 3 mm) coated with the samples as a working electrode. To prepare the working electrode, a suspension of 5 mg/mL of the carbon materials synthesized above was made in 2-propanol, and 1.4 μL of this suspension was then drop-casted onto the surface of a freshly polished glassy carbon disc electrode (GCE). The final catalyst loading was set as 100 $\mu g/cm^2$. After letting the catalyst-coated electrode dry under ambient condition, 2 μL of Nafion solution was drop-casted on the top of it. The electrode was allowed to dry completely, also under ambient condition, and it was then become ready to use.

Electrocatalytic ORR was performed using a 5 mm GCE and a Pine bipotentiostat (Pine Research Instrumentation). To make the comparison among the catalytic activities of the different materials easier, a similar amount of catalyst (100 $\mu g/cm^2$) was loaded or used on the working electrode for each electrocatalytic test. The scan rates for cyclic voltammetry (CV) and linear scan voltammetry (LSV) were used as 10 mV/s, unless mentioned otherwise. All the electrochemical measurements were performed at room temperature and ambient pressure. The potential vs SCE was converted to potential against the reversible hydrogen electrode (RHE) by using the equation $E_{vs\,RHE} = E_{vs\,SCE} + E^{\circ}_{SCE} + 0.059pH$.[57]

Additional electrochemical studies using a rotating ring-disk electrode were also performed, and based on the results the number of electrons transferred during ORR (n) was calculated with the equation[32]

$$n = 4 \times J_D/(J_D + J_R/N)$$

where J_D is the disk current, J_R is the ring current, and N is the collection efficiency of the Pt ring electrode. The percentage of hydrogen peroxide in the products ($\%H_2O_2$) produced by the ORR was calculated according to the equation

$$\%H_2O_2 = 200 \times J_R/(J_D \times N + J_R)$$

where again J_D is the disk current, J_R is the ring current, and N is the collection efficiency of the Pt ring electrode.

Characterization. Powder X-ray diffraction patterns of the materials were recorded with a Rigaku D/Max 2550 X-ray diffractometer operating at a wavelength (λ) = 0.154 05 nm of Cu

DOI: 10.1021/acsami.6b05739
ACS Appl. Mater. Interfaces 2016, 8, 18891−18903

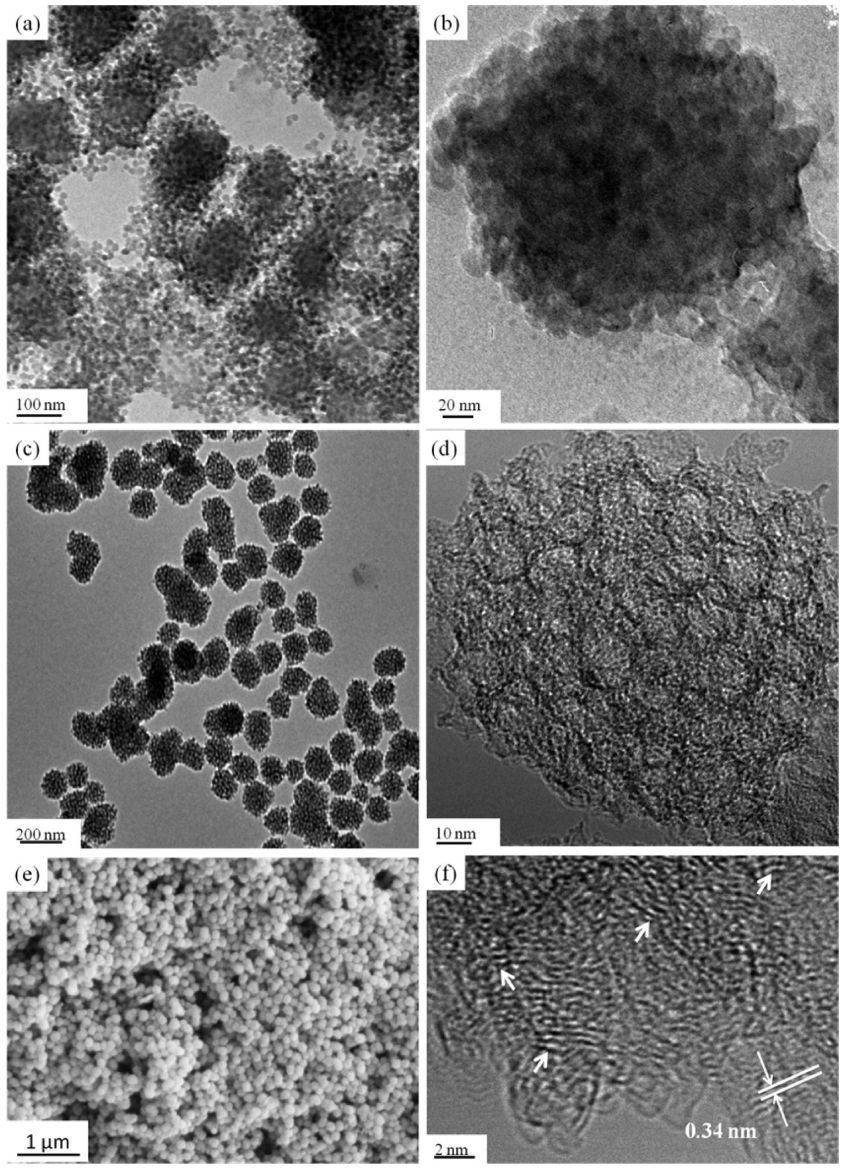

Figure 1. TEM images of spontaneously self-assembled PANI-SiO_2 nanocomposite material before pyrolysis (a, b) and the corresponding carbon material obtained after pyrolysis and removal of the colloidal silica from it (or PAMC-900) (c, d). SEM (e) and HRTEM (f) images of PAMC-900.

Kα radiation. The pore properties of the materials were investigated by physical adsorption of nitrogen at the liquid-nitrogen temperature (−196 °C) using a Micromeritics TriStar-3000 (Micromeritics, USA). Before each measurement, the sample was degassed for 6 h at 70 °C under nitrogen gas. The Brunauer−Emmett−Teller (BET) surface area and Barrett−Joyner−Halenda (BJH) pore size distribution of the materials were then determined from the adsorption/desorption data. Raman spectra were obtained using a Renishaw Raman spectrometer, model 1000, operating with a laser excitation light source (λ = 514.5 nm). The elemental composition of the PAMC and control materials was probed with a Thermo Scientific K-Alpha X-ray photoemission spectrometer (XPS) equipped with an Al Kα radiation as the X-ray source ($h\upsilon$ = 1486.6 eV). Field emission scanning electron microscope (FESEM) images of the materials were acquired using a Zeiss Sigma Field Emission SEM. Transmission electron microscopic (TEM) images of the materials were obtained with a Topcon 002B TEM microscope operating at 200 kV. High-resolution TEM images were obtained with a Tecnai G2 S-Twin F20 transmission electron microscope. Thermogravimetric analyses (TGA) of the PAMC and the relevant control materials were done with a PerkinElmer TGA7 instrument, by heating each sample at a rate of 10 °C/min under a constant flow of air at a rate of 20 mL/min.

RESULTS AND DISCUSSION

Heteroatom-doped polyaniline (PANI)-derived mesoporous carbon nanoparticles (PAMCs) are synthesized via three synthetic steps, as illustrated in Scheme 1. First, aniline is polymerized using $(NH_4)_2S_2O_8$ as oxidant in acidic solution in the presence of colloidal silica nanoparticle (12 nm) templates. After removing the solvent from the resulting solid product by evaporation, a PANI−silica nanocomposite material, denoted as PANI-SiO_2, is obtained. The composite material is treated under inert atmosphere (argon) at 300 °C for 3 h and then at 700, 800, 900, or 1000 °C for 2 h to carbonize the polymer in it. After removing the silica templates from the carbonized products by treating them with aqueous NaOH solution, heteroatom-doped PANI-derived mesoporous nanoparticles are obtained. The materials are denoted as PAMC-*T*, where *T* represents their final pyrolysis temperatures, namely 700, 800, 900, or 1000 °C (or they are called PAMC-700, PAMC-800, PAMC-900, and PAMC-1000, respectively).

DOI: 10.1021/acsami.6b05739
ACS Appl. Mater. Interfaces 2016, 8, 18891−18903

For comparative studies, three more materials are prepared by carbonizing at 900 °C three other precursors, namely (1) PANI-SiO_2-H_2O (PANI−silica nanocomposite material that is prepared using water instead of 1 M HCl as a solvent), (2) PANI-SiO_2-15 (which is made using less amount of solvent compared with the one used for making PANI-SiO_2), and (3) bulk PANI (which is synthesized without the presence of colloidal silica templates) (see Experimental Section for details). The SiO_2 templates in the first two materials are removed with aqueous NaOH solution. Three additional carbon materials, denoted as PAMC-900-H_2O, PAMC-900-15, and PANC-900, are finally obtained, and they are used as control samples for various parts of the studies.

The TEM image (Figure 1a) indicates that the polymerization of aniline in the presence of colloidal SiO_2 spontaneously forms PANI/colloidal SiO_2 composite materials having spherical morphology, just like related materials reported previously.[27,28] Besides the spherical PANI-SiO_2 aggregates, a few free silica nanoparticles are also observed in the images. Furthermore, the TEM images of the aggregates show that the PANI and SiO_2 are completely interwoven (Figures 1a,b). Moreover, the carbon products ultimately obtained from the PANI−colloidal SiO_2 nanocomposite materials by pyrolysis, followed by removal of their SiO_2 templates, generally have similar spherical morphology and nanoscale size as their precursors. For example, the TEM image of PAMC-900 (Figure 1c) shows mostly isolated mesoporous carbon nanoparticles, just like those in Figure 1. Moreover, the TEM image of the particles (Figures 1d) shows that the materials have nanoporous structures with an average pore size of ca. 12 nm. In addition, a closer observation by high-resolution TEM (HRTEM) (Figure 1f) reveals that PAMC-900 contains some amorphous carbon phase as well as some lattice fringes with an interlayer distance of 0.34 nm corresponding to graphitic carbon. The SEM image of PAMC-900 further reveals that the material possesses monodisperse carbon nanoparticles (Figure 1e). The materials prepared at pyrolysis temperatures other than 900 °C also show uniformly sized nanoparticles with similar spherical morphology and size (Figure 2) as the one obtained at 900 °C. However, when the synthesis of PANI with silica aggregates is done in water (i.e., with no HCl), the resulting carbon material (PAMC-900-H_2O) does not show particles with uniform morphology (Figure 3). These results suggest that the protonated PANI in PANI-SiO_2 formed due to the HCl present into the solution during the synthesis of the materials may have helped the PANI and SiO_2 to aggregate and form the observed spherical composite nanoparticles.[30]

Besides the type of solvent, the amount of solvent employed to make the PANI-SiO_2 precursors is found to affect the size of the carbon nanoparticles ultimately resulting from the synthesis. For example, when the total amount of solvent is 84 mL, the synthesis leads to carbon particles with a size of about 128 ± 12 nm (i.e., PAMC-900) (Figure 1e); however, when the total amount of solvent is decreased from 84 to 39 mL, the synthesis leads to larger and aggregated particles with an average size of 254 ± 37 nm (Figure S1). So, it is necessary to use the right amount of solvent in the reaction mixture to produce well-dispersed precursors and thereby isolated carbon nanoparticles in the end.

The nitrogen adsorption/desorption measurement of PAMC-900 (Figure S2) displays a type IV isotherm with some hysteresis loops, suggesting that the material has mesoporous structure. The material's BET surface area is 652 m^2/g (Table S2), and its BJH pore size distribution curve shows a sharp peak centered at ca. 12 nm. The same type of isotherm and a similar pore size distribution are also observed for the other PAMC materials synthesized under different pyrolysis temperatures (Figure S2), consistent with the TEM results discussed above. The similarity in pore structure of all the materials we have synthesized is an indirect indication that the colloidal silica particles used for the synthesis of the materials must have not only served as templates but also done so in a similar manner in all the cases. This is corroborated by the fact that PANC-900 (one of the control materials or the carbon material made at 900 °C from PANI without silica templates) is found to have barely any mesoporosity as can be seen on its nitrogen adsorption/desorption isotherm (Figure S2). Its BET surface area is also low (18 m^2/g). Its TEM and SEM images (Figure S3) indicate that the material has a very irregular morphology with no apparent porosity as well. So, based on the results above, the importance of the colloidal silica in producing carbon nanoparticles is undeniable, which is they allow the formation of carbon materials with more appealing (or porous) structure. The surface area and other pore properties of the PAMC materials and the control material PANC-900 are all summarized in Table S2.

The X-ray diffraction (XRD) patterns (Figure S4) of the PMAC materials display a strong, broad diffraction peak at 2θ of ca. 24° (002), which can be ascribed to the characteristic

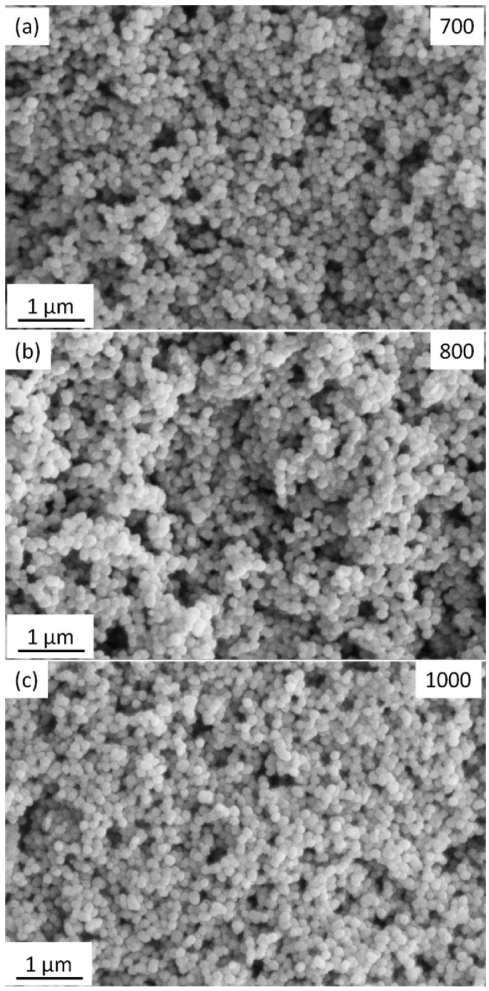

Figure 2. SEM images of the PAMC materials synthesized at different pyrolysis temperatures: (a) 700, (b) 800, and (c) 1000 °C.

DOI: 10.1021/acsami.6b05739
ACS Appl. Mater. Interfaces 2016, 8, 18891−18903

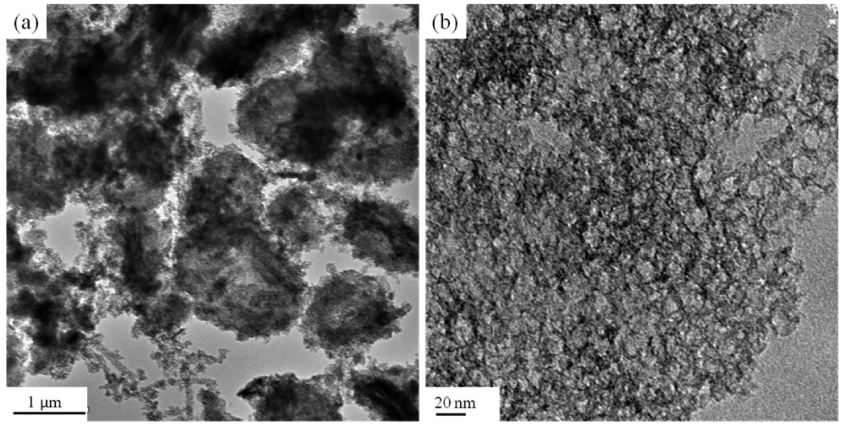

Figure 3. Low magnification (a) and high magnification (b) TEM images of PAMC-900-H_2O, which is synthesized using water as the main solvent and a pyrolysis temperature of 900 °C.

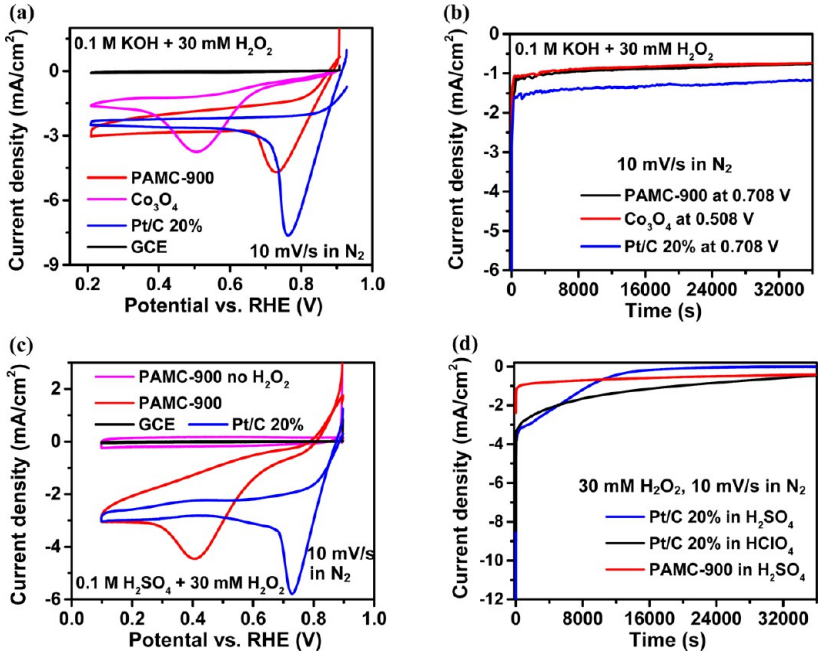

Figure 4. (a) Cyclic voltammograms (CVs) recorded for HPRR of 30 mM H_2O_2 in aqueous KOH solution (0.1 M) over PAMC-900, Co_3O_4, Pt/C (20 wt %), or blank GCE. (b) Chronoamperometry curves for electroreduction of 30 mM H_2O_2 in aqueous KOH solution (0.1 M) over PAMC-900 at 708 mV vs RHE (black curve), over Co_3O_4 at 508 mV vs RHE (red curve), and over Pt/C 20% at 708 mV vs RHE (blue curve). (c) CVs over PAMC-900 of 0 mM H_2O_2 in 0.1 M H_2SO_4 solution (magenta) and of 30 mM H_2O_2 in 0.1 M H_2SO_4 solution (red). The results over bare GCE and Pt/C (20 wt %) with 30 mM H_2O_2 in 0.1 M H_2SO_4 are also shown. (d) Chronoamperometry curves for HPRR of 30 mM H_2O_2 over PAMC-900 or Pt/C (20 wt %) in 0.1 M H_2SO_4 solution and over Pt/C (20 wt %) in 0.1 M $HClO_4$ at the potential of 0.5 V vs RHE.

crystalline structure formed by the sp^2-hybridized carbon atoms of graphitic materials. In addition, a weak signal at $2\theta = 44°$ (100), which can be attributed to the coherent and parallel stacking of graphitic sheets,[58] is observed.

This synthetic method used to make mesoporous carbon nanospheres using PANI as a precursor and silica nanoparticles as templates above is also successfully demonstrated to work for another nitrogen-containing polymer, PPY. The resulting material in the latter case is found to have equally well isolated mesoporous carbon nanoparticles, just like the ones seen in the PAMC materials (see its SEM image in Figure S5).

The electrocatalytic activity of PAMC-900 toward HPRR and ORR in KOH solution (0.1 M) is then examined, first by cyclic voltammetry (CV) (Figure 4a). The results show that the material efficiently catalyzes HPRR under basic condition, with a peak potential at 728 mV vs RHE. On the contrary, and as can be expected, the bare GCE produces no reduction current under similar condition, confirming that PAMC-900 must have been responsible for the HPRR obtained in the former case. As platinum is an efficient catalyst for numerous reactions,[47,51,59] including ORR as well as HPRR, we employed the commercially available Pt/C (20 wt %) as a reference to compare the electrocatalytic performance of the PAMC materials with. The peak potential at which HPRR occurs in basic solution (0.1 M NaOH) over PAMC-900 (728 mV vs RHE) is closer to the one obtained for Pt/C (762 mV vs RHE). Moreover, PAMC-900s catalytic activity is much better than that of Co_3O_4 (508 mV vs RHE), which is a commonly studied electrocatalyst for HPRR in alkaline solution. Additionally, when the stability of PAMC-900 is compared with Co_3O_4 using

DOI: 10.1021/acsami.6b05739
ACS Appl. Mater. Interfaces 2016, 8, 18891−18903

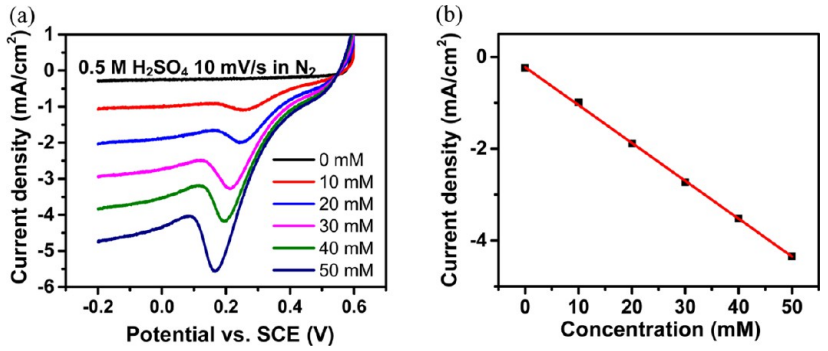

Figure 5. (a) Linear sweep voltammetry (LSV) curves HPRR over PAMC-900 recorded in solutions containing 0, 10, 20, 30, 40, and 50 mM H_2O_2 in 0.5 M H_2SO_4. (b) A plot showing current density at 0 V (vs SCE) as a function of concentration of H_2O_2. (Please note that some of the values of the potential are purposely recorded as "potential vs. SCE", or they not changed into "potential vs. RHE", in order to directly compare the results for PAMC with some pertinent onset potential values reported in "potential vs. SCE" for HPRR in the literature.)

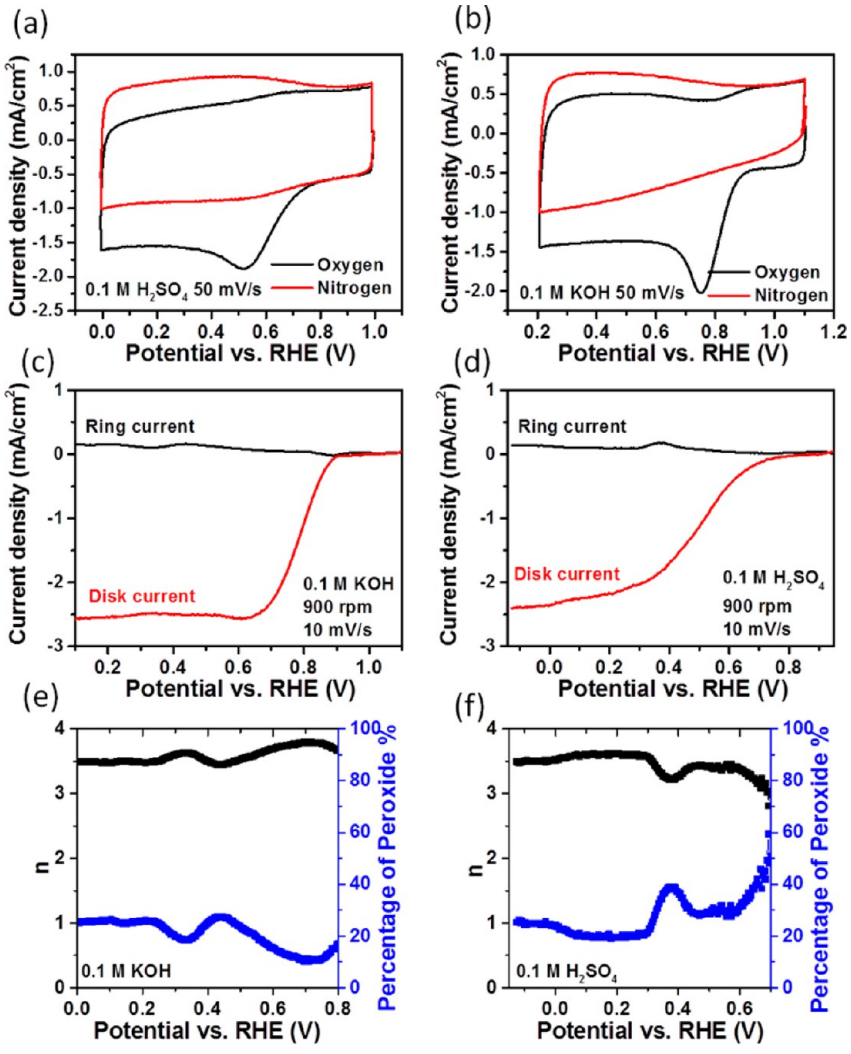

Figure 6. (a–d) CV and LSV curves obtained over PAMC-900 in O_2- or N_2-saturated acidic and basic solutions. The results include CV curves at a sweep rate of 50 mV/s over PAMC-900 in O_2- and N_2-saturated 0.1 M KOH solutions (a) and 0.1 M H_2SO_4 solutions (b). Also displayed are the LSV curves recorded at 900 rpm with 10 mV/s sweep rate over PAMC-900 in O_2-saturated 0.1 M KOH solution (c) and in O_2-saturated 0.1 M H_2SO_4 solution (d). The calculated number of electrons transferred or the percentage of H_2O_2 in the product versus applied potential during the HPRR in 0.1 M KOH solution (e) or in 0.1 M H_2SO_4 solution (f).

chronoamperometry for 10 h, PAMC-900 shows a reasonably stable reduction current at 708 mV vs RHE, but Co_3O_4 gives a similar current only at a potential of 508 mV vs RHE (or at a much higher overpotential) under the same conditions (Figure 4b). Overall, these results indicate that PAMC-900 is a more suitable and efficient electrocatalyst for HPRR, and it works well as electrocatalyst for this reaction at less overpotential in

DOI: 10.1021/acsami.6b05739
ACS Appl. Mater. Interfaces 2016, 8, 18891–18903

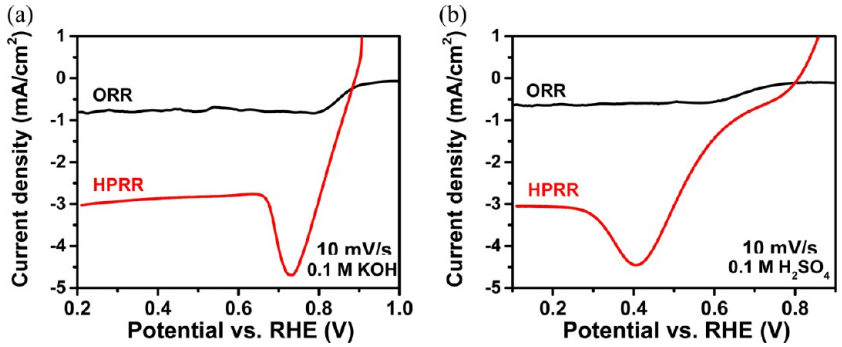

Figure 7. Comparison between the LSV curve of ORR (in O_2-saturated electrolyte) and that of HPRR (in 30 mM H_2O_2) over PAMC-900 catalyst in (a) 0.1 M KOH and (b) 0.1 M H_2SO_4 solutions.

basic medium than other commonly used electrocatalysts for the reaction.

As mentioned above, performing HPRR in acidic electrolyte can have an added advantage as it may allow the direct usage of the H_2O_2 that can be generated from oxygen (O2) through ORR with the aid of solar energy under acidic condition.[49] Moreover, as carbon materials are generally more stable under such condition, they are better suited to meet this goal than most metal-based catalysts, such as Co_3O_4, which are unstable under acidic condition.

To determine if this can be the case for PAMC materials, and also to evaluate their electrocatalytic properties in acidic solution, the catalytic activity of PAMC-900 for HPRR in 0.1 M H_2SO_4 is measured (Figure 4c). The CV of HPRR in 30 mM H_2O_2 in 0.1 M H_2SO_4 over PAMC-900 at a scan rate of 10 mV/s (red curve in Figure 4c) reveals an obvious reduction current with an onset potential at ca. 798 mV vs RHE and a peak current density of −4.45 mA/cm^2 at the potential of 407 mV vs RHE. On the contrary, no reduction current is detected when the CV is recorded in 0 mM H_2O_2 over the same catalyst, indicating that the observed current is exclusively due to HPRR. Similarly, no signal is observed in 30 mM H_2O_2 when the GCE contains no catalyst, further confirming PAMC-900's involvement as electrocatalyst in the HPRR. But the peak potential (and the corresponding overpotential) for the reaction over PAMC-900 in acidic solution is slightly inferior to that obtained in basic medium above. Furthermore, the linear sweep voltammograms (LSV) over PAMC-900 in 0.5 M H_2SO_4 containing different concentrations of H_2O_2 reveals that the reduction current density increases linearly as the concentration of H_2O_2 is increased (Figure 5).

Next, the electrocatalytic activity of PAMCs in acidic solution is compared with that of other notable materials under similar conditions. Compared with nanoporous gold leaves, whose onset potential for HPRR is reported to be of 95 mV vs SCE in 10 mM H_2O_2,[41] PAMC-900 gives a much better onset potential of 550 mV vs SCE (or a much less overpotential) for the reaction under the same condition. Although PAMC-900 shows less electrocatalytic activity in the beginning of the reaction than Pt/C (20 wt %) (Figure 4c), the former remains more stable over long-term operation (Figure 4d). This is also corroborated by experimental results obtained with chronoamerometry, which shows that the residual current density of HPRR over PAMC-900 is relatively more stable than that over Pt/C (Figure S6). Pt/C's relatively faster loss of catalytic activity in HPRR, compared with PAMC, under this condition is actually not surprising, and is most likely to do with Pt's higher tendency to undergo surface oxidation in acidic H_2O_2 solution. In fact, given the standard reduction potentials for HPRR in aqueous acidic and basic solutions are 1.776 and 0.878 V, respectively, the ability of H_2O_2 to oxidize others (i.e., Pt in this case) is stronger in acidic solution.[60] This is also consistent with a report on the conversion of Pt to Pt−OH during HPRR.[61] In addition, possible adsorption of sulfate ions onto Pt from the electrolyte (or the H_2SO_4 we used) may have also contributed to Pt's loss of activity,[62] since we have found that Pt/C's electrocatalytic activity is slightly better in 0.1 M $HClO_4$ than in 0.1 M H_2SO_4. Nevertheless, the carbon nanomaterials reported herein seem to suffer less from these issues.

Given recent reports on the ability of carbon materials to electrocatalyze ORR,[31−39] additional experiments are performed to determine this scenario for PAMC materials. As shown in Figures 6a and 6b, while no peak current is observed when PAMC-900 is used as an electrocatalyst in N_2-saturated KOH (0.1 M) and H_2SO_4 (0.1 M) solutions, an obvious peak is observed after bubbling O_2 into the electrolytes. This clearly indicates that PAMC-900 can effectively electrocatalyze ORR. This is further confirmed by an experiment done using a rotating disk electrode (RDE), in which PAMC is once again seen to electrocatalyze ORR (Figures 6c,d). Based on the ring current and disk current, the number of electrons transferred during ORR in aqueous KOH solution (0.1 M) is determined to be between 3.5 and 4.0, suggesting that ORR proceeds primarily through a 4-electron pathway. Accordingly, the reaction gives mainly H_2O or only a small amount (ca. 20%) H_2O_2 product. On the other hand, the percentage of H_2O_2 formed in the ORR is slightly higher in H_2SO_4 solution (0.1 M). Moreover, the amount H_2O_2 formed in the reactions varies with the applied potential, and this variation is more in acidic solution than in basic solution.

HPRR is known to go through a direct or an indirect pathway. The direct pathway involves a 2-electron process as $H_2O_2 + 2H^+ + 2e^- = 2H_2O$, and the indirect pathway proceeds through the chemical decomposition of H_2O_2 to O_2, followed by ORR as $O_2 + 4H^+ + 4e^- = 2H_2O$. To assess which pathway the HPRR goes through over PAMC, first the electrocatalytic ORR test over the PAMC-900 in H_2SO_4 (0.1 M) is assessed. The current density obtained for ORR at 0 rpm at 200 mV vs RHE is −0.62 mA/cm^2, which is much lower than the one obtained for HPRR in the presence of 30 mM H_2O_2 at 0 rpm at the same potential (−3.27 mA/cm^2) (Figure 7a). If we assume that the HPRR proceeds via an indirect pathway, the current should be only due to the ORR, and its value should be close to or smaller than the one obtained for ORR in O_2-saturated electrolyte. However, this is found to be not the case, as the

DOI: 10.1021/acsami.6b05739
ACS Appl. Mater. Interfaces 2016, 8, 18891−18903

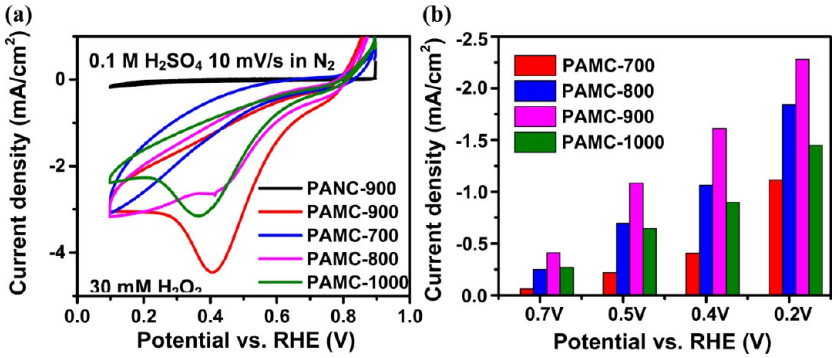

Figure 8. (a) CV curves recorded for 30 mM H_2O_2 in 0.1 M H_2SO_4 over PAMC-900, PANC-900, PAMC-700, PAMC-800, and PAMC-1000. (b) Comparison of steady state current density values obtained with chronoamperometry at various potentials over the different materials in 0.1 M H_2SO_4 for 5 min.

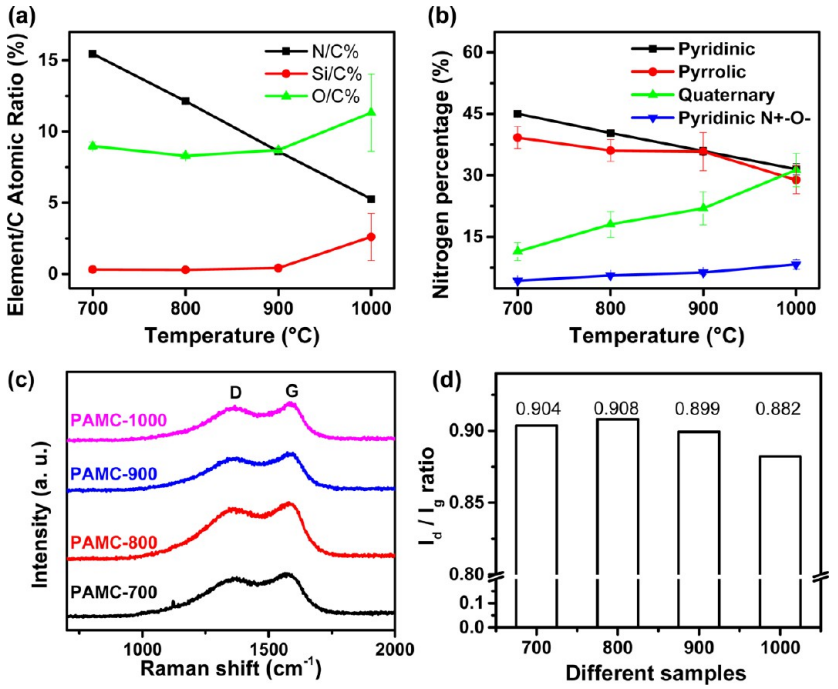

Figure 9. Compositions of PAMC-*T* materials as a function of pyrolysis temperature: (a) atomic percent ratios of N/C, O/C, and Si/C and (b) atomic percentages of different N species. (c) Raman spectra of PAMC-T materials. (d) I_d/I_g ratios for PAMC-T.

reduction current of HPRR is much larger than that of ORR over PAMC-900. These results then suggest that the HPRR over PAMC in acidic solution takes place via the direct pathway. A similar experimental process is previously applied to determine the HPRR pathways over cobalt oxide electrocatalyst.[45]

Additionally, LSV curves over the PAMC materials in O_2-saturated aqueous KOH electrolyte (0.1 M) are obtained. As shown in Figure 7b, the limiting current density of the reaction is less than 1 mA/cm^2, which is a much smaller value than the one obtained for HPRR over the same material (whose limiting current density is ca. 3 mA/cm^2). This result confirms that the HPRR over the PAMC in basic solution goes mainly through the direct route.

Next, the electrocatalytic activity toward HPRR of the PAMC materials prepared at temperatures other than 900 °C and the control material PANC-900 is investigated. Based on the CV results obtained for the materials (Figure 8a), not surprisingly PANC-900 is seen to exhibit negligible electrocatalytic activity, most likely due to its lack of mesoporosity and high surface area, whereas all the PAMC materials show some activity. The electrocatalytic activity of the latter materials toward HPRR is found to be in the order of PAMC-700 < PAMC-800 ≈ PAMC-1000 < PAMC-900. This trend is further confirmed by steady state current density measurements for 5 min at 0.5 V vs RHE (see Figure S7). Results of additional experiments at different potentials (0.7, 0.5, 0.4, and 0.2 V vs RHE) (Figure 8b) indicate that among the materials we have investigated here, PAMC-900 is the best electrocatalyst for HPRR.

To get some insights into the reasons behind the observed differences in electrocatalytic activity, the compositions of the materials are studied by X-ray photoelectron spectroscopy (XPS). Based on the XPS survey spectra (Figure S8), the PAMC materials are found to contain mainly C, O, N, and Si. The atomic percent ratio of N/C is found to decrease significantly when the pyrolysis temperature is increased (Figure 9a). The high-resolution XPS spectra of C 1s further

DOI: 10.1021/acsami.6b05739
ACS Appl. Mater. Interfaces 2016, 8, 18891−18903

indicate the presence of nitrogen dopant in the materials (Figure S10). The high-resolution XPS spectra for N 1s can be fitted into four peaks with different binding energy values of 398.1, 400.0, 400.9, and 403.5 eV, corresponding to the pyridinic, pyrrolic, quaternary, and pyridinic N^+-O^- nitrogen groups, respectively (Figure S9). Notably, the percentage of quaternary nitrogen species in the materials, which are often indicative of higher degree of graphitization in carbon materials, increases as the pyrolysis temperature is increased (Figure 9b). On the other hand, the atomic ratios of O/C and Si/C in the PAMC materials obtained at different temperatures are found to be very similar (Figure 9a), implying that the majority of O and Si must have been originated from the same precursor, which is only likely to be the SiO_2 templates. Upon analyzing the high resolution XPS spectrum of Si 2p, the material is found to contain primarily SiO_xC_y species (102.1 eV) (Figure S11).[63] This indicates that the high temperature pyrolysis treatment of PANI-SiO_2 leads to the partial reduction of SiO_2 to SiO_xC_y.

To determine why PAMC-1000 shows less electrocatalytic activity than PAMC-900, the two materials are analyzed by thermogravimetryic analysis (TGA) in air (Figure S12). The results indicate that PAMC-1000 produces a lot more residue (ca. 64%) than PAMC-900 does (only ca. 0.5%). This indicates that the former generally possesses much more silicon/silica ("noncombustible") species. However, the XPS spectrum of PAMC-1000 indicates that this material has very little (2.2 ± 1.3%) silicon species (Figure S13). On the other hand, the XPS spectrum of the same material after calcination at 900 °C in air for 30 min (a condition that can remove the carbon in the material) shows a lot more Si species (17.7 ± 1.2%). It should be noted here that the content of silica/silicon species determined by TGA is generally much higher than the ones obtained by XPS because the entire material's composition is subject to analysis by the former while only/mainly the surface composition is inherently analyzed by the latter. So, these results indicate that most of the Si species in PAMC-1000 are not on the surface of the PAMC materials but are rather embedded within the carbon materials.

Hence, we believe that the much higher amount of silica or silicon species in the form of SiO_xC_y present in PAMC-1000 may have caused PAMC-1000 to show less electrocatalytic activity toward HPRR compared with PAMC-900. This is in turn because the increase in the relative amount of SiO_xC_y and related species compromises the electrical conduction and electron transfer processes in the material.[64] Besides this, PAMC-1000s lower surface area compared with PAMC-900s (Table S2) may have also been partly the reason behind the lower electrocatalytic activity exhibited by the former.

In order to confirm the importance of nitrogen dopant in the carbon material for HPRR, another mesoporous carbon material is synthesized by using poly(fufuryl alcohol) as precursor under otherwise similar synthetic conditions as the one used to make PAMC-900. The resulting material, which is denoted as FAMC-900, also possesses a relatively high BET surface area (522 m^2/g) as PAMC-900 but with no nitrogen dopants in it (Figure S14). CV results in aqueous H_2SO_4 solution (0.1 M) with 30 mM H_2O_2 (Figure S15) reveal that this material gives negligible current density compared with PAMC-900, indicating the importance of N dopants in the electrocatalytic activity of these materials toward HPRR.

However, besides the N dopants, there must have been additional factors that influence the electrocatalytic activity of the PAMC materials. This is because the PAMC materials exhibit increased electrocatalytic activity as their pyrolysis temperature is increased from 700 to 900 °C or while their nitrogen dopant content decreases. Further investigation of all PAMC materials by Raman spectroscopy gives spectra with two peaks, at ca. 1350 and 1580 cm^{-1} (Figure 9c), which correspond to the D and G bands, respectively, of graphitic carbon. While the D peak stems from the hybridized vibrational mode related with the disorder or defect band in carbon material, the G peak is often associated with the tangential oscillations/vibrations of the sp^2 carbon atoms in the material.[57] More importantly, the I_d/I_g ratio of the PAMC materials prepared at different pyrolysis temperatures does not reveal significant variation (Figure 9d), suggesting that all the materials contain a similar proportion of defect sites, regardless of what causes them (i.e., the presence of N atoms or vacancy sites in the material).[39,65] If the presence of N dopants causes the structural defects, then a decreasing trend in the I_d/I_g ratio would have been observed upon increasing their pyrolysis temperature. However, this is found to be not the case; i.e., the N dopant atoms decrease significantly, but the I_d/I_g ratio remains the same as the pyrolysis temperature is increased. This implies that some vacancy related of defect sites must have formed and existed in the structure of the carbon materials to keep the same, high I_d/I_g ratio as the pyrolysis temperature is increased. Recently, it was reported that such kinds of vacancy-related defect sites could not only be created by the formation of interstitial vacancy in the structures of carbon materials but also be responsible to carbon materials' electrocatalytic activity in different reactions.[39,65] So, we believe that PAMC-900's higher electrocatalytic activity toward HPRR, compared with PAMC-800's and PAMC-700's, must be partly due to the presence of relatively higher amount of intrinsic vacancy-related defect sites in the former.

On the basis of the results presented above, we propose a plausible mechanism for the catalytic process of HPRR over the PAMC materials (Scheme 2). First, we believe that the defects

Scheme 2. Schematic Representation of the Proposed Electrocatalytic Processes during HPRR over PAMC Material

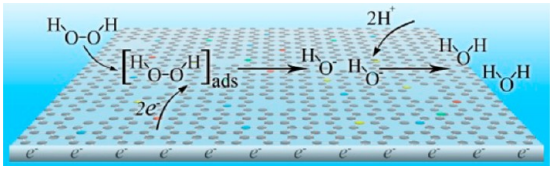

formed in the structure of PAMC, due to heteroatom dopants (mainly nitrogen) and vacancy sites, create electronically modulated (i.e., electron rich and electron poor) sites that can promote H_2O_2's interaction with the materials, in the same way as one reported for O_2's interaction with heteroatom-doped carbon materials during ORR.[66] Then, a charge transfer from the catalyst to the oxygen atoms of H_2O_2 occurs, weakening the O−O bond in H_2O_2 molecule, a process that is considered to be the rate-determining step in HPRR.[67,68] Finally, we believe that the resulting, activated H_2O_2 molecule with a weakened O−O bond easily undergoes the electrochemical reduction by accepting electrons.

DOI: 10.1021/acsami.6b05739
ACS Appl. Mater. Interfaces 2016, 8, 18891−18903

CONCLUSIONS

In summary, we have successfully synthesized monodisperse, mesoporous carbon nanoparticles (PAMCs) from polymer/colloidal silica self-aggregates using a facile synthetic route. The materials have been demonstrated to serve as effective electrocatalysts for the hydrogen peroxide reduction reaction (HPRR) and the oxygen reduction reaction (ORR), in both acidic and alkaline solutions. It has been found that the materials show good electrocatalytic activity because of the heteroatom dopants/the defect sites present in their structures, their high porosity, and their high surface area. The materials' electrocatalytic activity has been found to be better than the few metal-based materials reported to catalyze HPRR (such as nanoporous Au and Co_3O_4). The PAMC materials have also been found to be more stable electrocatalysts in HPRR in acidic condition than conventional metal-based electrocatalysts. Additionally, the work has provided insights into the effects of heteroatom dopants on carbon materials on their catalytic properties toward HPRR. The findings can encourage further investigation of other carbon-based, metal-free materials for electrocatalysis of HPRR, a reaction that is relatively underexplored.

ASSOCIATED CONTENT

Supporting Information

The Supporting Information is available free of charge on the ACS Publications website at DOI: 10.1021/acsami.6b05739.

Additional characterization results, including electron microscopy images, X-ray diffraction patterns, X-ray photoelectron spectra, and electrochemical data and curves (PDF)

AUTHOR INFORMATION

Corresponding Authors

*E-mail: xxzou@jlu.edu.cn (X.Z.).
*E-mail: tasefa@rci.rutgers.edu (T.A.).

Notes

The authors declare no competing financial interest.

ACKNOWLEDGMENTS

T.A. acknowledges the financial support of the National Science Foundation in the US (NSF 1508611 and NSF 1134289). X.Z. appreciates financial assistance from the National Science Foundation of China (NSFC 21401066) and Jilin Province Science and Technology Development Project (20150520003JH).

REFERENCES

(1) Liu, J.; Wickramaratne, N. P.; Qiao, S. Z.; Jaroniec, M. Molecular-Based Design and Emerging Applications of Nanoporous Carbon Spheres. *Nat. Mater.* **2015**, *14*, 763−774.
(2) Liang, C.; Li, Z.; Dai, S. Mesoporous Carbon Materials: Synthesis and Modification. *Angew. Chem., Int. Ed.* **2008**, *47*, 3696−3717.
(3) Chen, Y.; Shi, J. Mesoporous Carbon Biomaterials. *Sci. China Mater.* **2015**, *58*, 241−257.
(4) Tang, J.; Liu, J.; Li, C.; Li, Y.; Tade, M. O.; Dai, S.; Yamauchi, Y. Synthesis of Nitrogen-Doped Mesoporous Carbon Spheres with Extra-Large Pores through Assembly of Diblock Copolymer Micelles. *Angew. Chem., Int. Ed.* **2015**, *54*, 588−593.
(5) Qiao, Z.-A.; Guo, B.; Binder, A. J.; Chen, J.; Veith, G. M.; Dai, S. Controlled Synthesis of Mesoporous Carbon Nanostructures via a "Silica-Assisted" Strategy. *Nano Lett.* **2013**, *13*, 207−212.
(6) Kim, T.-W.; Chung, P.-W.; Slowing, I. I.; Tsunoda, M.; Yeung, E. S.; Lin, V. S.-Y. Structurally Ordered Mesoporous Carbon Nanoparticles as Transmembrane Delivery Vehicle in Human Cancer Cells. *Nano Lett.* **2008**, *8*, 3724−3727.
(7) Gu, J.; Su, S.; Li, Y.; He, Q.; Shi, J. Hydrophilic Mesoporous Carbon Nanoparticles as Carriers for Sustained Release of Hydrophobic Anti-Cancer Drugs. *Chem. Commun.* **2011**, *47*, 2101−2103.
(8) Sun, Z.; Liu, Y.; Li, B.; Wei, J.; Wang, M.; Yue, Q.; Deng, Y.; Kaliaguine, S.; Zhao, D. General Synthesis of Discrete Mesoporous Carbon Microspheres through a Confined Self-Assembly Process in Inverse Opals. *ACS Nano* **2013**, *7*, 8706−8714.
(9) White, R. J.; Tauer, K.; Antonietti, M.; Titirici, M.-M. Functional Hollow Carbon Nanospheres by Latex Templating. *J. Am. Chem. Soc.* **2010**, *132*, 17360−17363.
(10) Liu, R.; Mahurin, S. M.; Li, C.; Unocic, R. R.; Idrobo, J. C.; Gao, H.; Pennycook, S. J.; Dai, S. Dopamine as a Carbon Source: The Controlled Synthesis of Hollow Carbon Spheres and Yolk-Structured Carbon Nanocomposites. *Angew. Chem., Int. Ed.* **2011**, *50*, 6799−6802.
(11) Valle-Vigón, P.; Sevilla, M.; Fuertes, A. B. Synthesis of Uniform Mesoporous Carbon Capsules by Carbonization of Organosilica Nanospheres. *Chem. Mater.* **2010**, *22*, 2526−2533.
(12) Mezzavilla, S.; Baldizzone, C.; Mayrhofer, K. J. J.; Schuth, F. General Method for the Synthesis of Hollow Mesoporous Carbon Spheres with Tunable Textural Properties. *ACS Appl. Mater. Interfaces* **2015**, *7*, 12914−12922.
(13) Hampsey, J. E.; Hu, Q.; Wu, Z.; Rice, L.; Pang, J.; Lu, Y. Templating Synthesis of Ordered Mesoporous Carbon Particles. *Carbon* **2005**, *43*, 2977−2982.
(14) Liu, C.; Wang, J.; Li, J.; Luo, R.; Shen, J.; Sun, X.; Han, W.; Wang, L. Controllable Synthesis of Functional Hollow Carbon Nanostructures with Dopamine As Precursor for Supercapacitors. *ACS Appl. Mater. Interfaces* **2015**, *7*, 18609−18617.
(15) Liu, J.; Yang, T.; Wang, D.-W.; Lu, G. Q.; Zhao, D.; Qiao, S. Z. A Facile Soft-Template Synthesis of Mesoporous Polymeric and Carbonaceous Nanospheres. *Nat. Commun.* **2013**, *4*, 2798.
(16) Fang, Y.; Gu, D.; Zou, Y.; Wu, Z.; Li, F.; Che, R.; Deng, Y.; Tu, B.; Zhao, D. A Low-Concentration Hydrothermal Synthesis of Biocompatible Ordered Mesoporous Carbon Nanospheres with Tunable and Uniform Size. *Angew. Chem., Int. Ed.* **2010**, *49*, 7987−7991.
(17) Yang, Z.-C.; Zhang, Y.; Kong, J.-H.; Wong, S. Y.; Li, X.; Wang, J. Hollow Carbon Nanoparticles of Tunable Size and Wall Thickness by Hydrothermal Treatment of α-Cyclodextrin Templated by F127 Block Copolymers. *Chem. Mater.* **2013**, *25*, 704−710.
(18) Wang, S.; Li, W.-C.; Hao, G.-P.; Hao, Y.; Sun, Q.; Zhang, X.-Q.; Lu, A.-H. Temperature-Programmed Precise Control over the Sizes of Carbon Nanospheres Based on Benzoxazine Chemistry. *J. Am. Chem. Soc.* **2011**, *133*, 15304−15307.
(19) Wang, G.-H.; Sun, Q.; Zhang, R.; Li, W.-C.; Zhang, X.-Q.; Lu, A.-H. Weak Acid-Base Interaction Induced Assembly for the Synthesis of Diverse Hollow Nanospheres. *Chem. Mater.* **2011**, *23*, 4537−4542.
(20) Liu, J.; Qiao, S. Z.; Liu, H.; Chen, J.; Orpe, A.; Zhao, D.; Lu, G. Q. Extension of The Stöber Method to the preparation of Monodisperse Resorcinol-Formaldehyde Resin Polymer and Carbon Spheres. *Angew. Chem., Int. Ed.* **2011**, *50*, 5947−5951.
(21) Zhao, J.; Niu, W.; Zhang, L.; Cai, H.; Han, M.; Yuan, Y.; Majeed, S.; Anjum, S.; Xu, G. A Template-Free and Surfactant-Free Method for High-Yield Synthesis of Highly Monodisperse 3-Aminophenol-Formaldehyde Resin and Carbon Nano/Microspheres. *Macromolecules* **2013**, *46*, 140−145.
(22) You, L.-J.; Xu, S.; Ma, W.-F.; Li, D.; Zhang, Y.-T.; Guo, J.; Hu, J. J.; Wang, C.-C. Ultrafast Hydrothermal Synthesis of High Quality Magnetic Core Phenol-Formaldehyde Shell Composite Microspheres Using the Microwave Method. *Langmuir* **2012**, *28*, 10565−10572.
(23) Choma, J.; Jamioła, D.; Augustynek, K.; Marszewski, M.; Gao, M.; Jaroniec, M. New Opportunities in Stöber Synthesis: Preparation of Microporous and Mesoporous Carbon Spheres. *J. Mater. Chem.* **2012**, *22*, 12636−12642.

(24) Silva, R.; Voiry, D.; Chhowalla, M.; Asefa, T. Efficient Metal-Free Electrocatalysts for Oxygen Reduction: Polyaniline-Derived N- and O-Doped Mesoporous Carbons. *J. Am. Chem. Soc.* **2013**, *135*, 7823−7826.
(25) Liang, H. W.; Wei, W.; Wu, Z. S.; Feng, X.; Müllen, K. Mesoporous Metal-Nitrogen-Doped Carbon Electrocatalysts for Highly Efficient Oxygen Reduction Reaction. *J. Am. Chem. Soc.* **2013**, *135*, 16002−16005.
(26) Wu, G.; More, K. L.; Johnston, C. M.; Zelenay, P. High-Performance Electrocatalysts for Oxygen Reduction Derived from Polyaniline, Iron, and Cobalt. *Science* **2011**, *332*, 443−447.
(27) Gill, M.; Mykytiuk, J.; Armes, S. P.; Edwards, J. L.; Yeates, T.; Moreland, P. J.; Mollett, C. Novel Colloidal Polyaniline-Silica Composites. *J. Chem. Soc., Chem. Commun.* **1992**, 108−109.
(28) Gill, M.; Armes, S. P. Particle Size Distributions of Polyaniline-Silica Colloidal Composites. *Langmuir* **1992**, *8*, 2178−2182.
(29) Maeda, S.; Armes, S. P. Preparation and Characterisation of Novel Polypyrrole-Silica Colloidal Nanocomposites. *J. Mater. Chem.* **1994**, *4*, 935−942.
(30) Wang, G.; Sun, Y.; Li, D.; Liang, H. W.; Dong, R.; Feng, X.; Müllen, K. Controlled Synthesis of N-Doped Carbon Nanospheres with Tailored Mesopores through Self-Assembly of Colloidal Silica. *Angew. Chem., Int. Ed.* **2015**, *54*, 15191−15196.
(31) Jiao, Y.; Zheng, Y.; Jaroniec, M.; Qiao, S. Z. Design of Electrocatalysts for Oxygen- and Hydrogen-Involving Energy Conversion Reactions. *Chem. Soc. Rev.* **2015**, *44*, 2060−2086.
(32) Meng, Y.; Voiry, D.; Goswami, A.; Zou, X.; Huang, X.; Chhowalla, M.; Liu, Z.; Asefa, T. N-, O-, and S-Tridoped Nanoporous Carbons as Selective Catalysts for Oxygen Reduction and Alcohol Oxidation Reactions. *J. Am. Chem. Soc.* **2014**, *136*, 13554−13557.
(33) Gong, Y.; Fei, H.; Zou, X.; Zhou, W.; Yang, S.; Ye, G.; Liu, Z.; Peng, Z.; Lou, J.; Vajtai, R.; Yakobson, B. I.; Tour, J. M. Boron- and Nitrogen-Substituted Graphene Nanoribbons as Efficient Catalysts for Oxygen Reduction Reaction. *Chem. Mater.* **2015**, *27*, 1181−1186.
(34) Huang, X.; Zou, X.; Meng, Y.; Mikmeková, E.; Chen, H.; Voiry, D.; Goswami, A.; Chhowalla, M.; Asefa, T. Yeast Cells-Derived Hollow Core/Shell Heteroatom-Doped Carbon Microparticles for Sustainable Electrocatalysis. *ACS Appl. Mater. Interfaces* **2015**, *7*, 1978−1986.
(35) Byon, H. R.; Suntivich, J.; Shao-Horn, Y. Graphene-Based NonNoble-Metal Catalysts for Oxygen Reduction Reaction in Acid. *Chem. Mater.* **2011**, *23*, 3421−3428.
(36) Zhou, R.; Qiao, S. Z. Silver/Nitrogen-Doped Graphene Interaction and Its Effect on Electrocatalytic Oxygen Reduction. *Chem. Mater.* **2014**, *26*, 5868−5873.
(37) Unni, S. M.; Illathvalappil, R.; Bhange, S. N.; Puthenpediakkal, H.; Kurungot, S. Carbon Nanohorn-Derived Graphene Nanotubes as a Platinum-Free Fuel Cell Cathode. *ACS Appl. Mater. Interfaces* **2015**, *7*, 24256−24264.
(38) Sa, Y. J.; Park, C.; Jeong, H. Y.; Park, S.-H.; Lee, Z.; Kim, K. T.; Park, G.-G.; Joo, S. H. Carbon Nanotubes/Heteroatom-Doped Carbon Core-Sheath Nanostructures as Highly Active, Metal-Free Oxygen Reduction Electrocatalysts for Alkaline Fuel Cells. *Angew. Chem., Int. Ed.* **2014**, *53*, 4102−4106.
(39) Zhang, J.; Zhao, Z.; Xia, Z.; Dai, L. A Metal-Free Bifunctional Electrocatalyst for Oxygen Reduction and Oxygen Evolution Reactions. *Nat. Nanotechnol.* **2015**, *10*, 444−452.
(40) Shaegh, S. A. M.; Nguyen, N.-T.; Ehteshami, S. M. M.; Chan, S. H. Amembraneless Hydrogen Peroxide Fuel Cell Using Prussian Blue as Cathode Material. *Energy Environ. Sci.* **2012**, *5*, 8225−8228.
(41) Yan, X.; Meng, F.; Xie, Y.; Liu, J.; Ding, Y. Direct N_2H_4/H_2O_2 Fuel Cells Powered by Nanoporous Gold Leaves. *Sci. Rep.* **2012**, *2*, 941.
(42) Zeis, R.; Lei, T.; Sieradzki, K.; Snyder, J.; Erlebacher, J. Catalytic Reduction of Oxygen and Hydrogen Peroxide by Nanoporous Gold. *J. Catal.* **2008**, *253*, 132−138.
(43) Miah, M. R.; Ohsaka, T. Kinetics of Electroreduction of H_2O_2 at gold electrodes in Iodide-Containing Alkaline Media. *J. Electrochem. Soc.* **2007**, *154*, F186−F190.
(44) Stewart, K. L.; Gewirth, A. A. Mechanism of Electrochemical Reduction of Hydrogen Peroxide on Copper in Acidic Sulfate Solution. *Langmuir* **2007**, *23*, 9911−9918.
(45) Cao, D.; Chao, J.; Sun, L.; Wang, G. Catalytic Behavior of Co_3O_4 in Electroreduction of H_2O_2. *J. Power Sources* **2008**, *179*, 87−91.
(46) Ke, X.; Xu, Y.; Yu, C.; Zhao, J.; Cui, G.; Higgins, D.; Chen, Z.; Li, Q.; Xu, H.; Wu, G. Pd-Decorated Three-Dimensional Nanoporous Au/Ni Foam Composite Electrodes for H_2O_2 Reduction. *J. Mater. Chem. A* **2014**, *2*, 16474−16479.
(47) Cui, C.-H.; Li, H.-H.; Yu, J.-W.; Gao, M.-H.; Yu, S.-H. Ternary Heterostructured Nanoparticle Tubes: A Dual Catalyst and Its Synergistic Enhancement Effects for O_2/H_2O_2 Reduction. *Angew. Chem., Int. Ed.* **2010**, *49*, 9149−9152.
(48) Kim, J.; Gewirth, A. A. Electrocatalysis of Peroxide Reduction by Au-Stabilized, Fe-Containing Poly(vinylpyridine) Films. *J. Phys. Chem. B* **2005**, *109*, 9684−9690.
(49) Yamada, Y.; Fukunishi, Y.; Yamazaki, S.; Fukuzumi, S. Hydrogen Peroxide as Sustainable Fuel: Electrocatalysts for Production with a Solar Cell and Decomposition with a Fuel Cell. *Chem. Commun.* **2010**, *46*, 7334−7336.
(50) Wu, K. H.; Wang, D. W.; Su, D. S.; Gentle, I. R. A Discussion on the Activity Origin in Metal-Free Nitrogen-Doped Carbons for Oxygen Reduction Reaction and Their Mechanisms. *ChemSusChem* **2015**, *8*, 2772−2788.
(51) Katsounaros, I.; Schneider, W. B.; Meier, J. C.; Benedikt, U.; Biedermann, P. U.; Auer, A. A.; Mayrhofer, K. J. J. Hydrogen Peroxide Electrochemistry on Platinum: Towards Understanding the Oxygen Reduction Reaction Mechanism. *Phys. Chem. Chem. Phys.* **2012**, *14*, 7384−7391.
(52) Kim, H.; Lee, K.; Woo, S. I.; Jung, Y. On the Mechanism of Enhanced Oxygen Reduction Reaction in Nitrogen-Doped Graphene Nanoribbons. *Phys. Chem. Chem. Phys.* **2011**, *13*, 17505−17510.
(53) Odedairo, T.; Yan, X.; Ma, J.; Jiao, Y.; Yao, X.; Du, A.; Zhu, Z. Nanosheets Co_3O_4 Interleaved with Graphene for Highly Efficient Oxygen Reduction. *ACS Appl. Mater. Interfaces* **2015**, *7*, 21373−21380.
(54) Shao, M. H.; Huang, T.; Liu, P.; Zhang, J.; Sasaki, K.; Vukmirovic, M. B.; Adzic, R. R. Palladium Monolayer and Palladium Alloy Electrocatalysts for Oxygen Reduction. *Langmuir* **2006**, *22*, 10409−10415.
(55) Fellinger, T. P.; Hasché, F.; Strasser, P.; Antonietti, M. Mesoporous Nitrogen-Doped Carbon for the Electrocatalytic Synthesis of Hydrogen Peroxide. *J. Am. Chem. Soc.* **2012**, *134*, 4072−4075.
(56) Liu, Y.; Quan, X.; Fan, X.; Wang, H.; Chen, S. High-Yield Electrosynthesis of Hydrogen Peroxide from Oxygen Reduction by Hierarchically Porous Carbon. *Angew. Chem., Int. Ed.* **2015**, *54*, 6837−6841.
(57) Zou, X.; Huang, X.; Goswami, A.; Silva, R.; Sathe, B.; Asefa, T. Cobalt-Embedded Nitrogen-Rich Carbon Nanotubes Efficiently Catalyze Hydrogen Evolution Reaction at All pH Values. *Angew. Chem.* **2014**, *126*, 4461−4465.
(58) Chaudhari, N. K.; Song, M. Y.; Yu, J. S. Heteroatom-Doped Highly Porous Carbon From Human Urine. *Sci. Rep.* **2014**, *4*, 5221.
(59) Qi, C.; Cong, H.; Cahill, K. J.; Müller, P.; Johnson, R. P.; Porco, J. A. Biomimetic Dehydrogenative Diels−Alder Cycloadditions: Total Syntheses of Brosimones A and B. *Angew. Chem., Int. Ed.* **2013**, *52*, 8345−8348.
(60) Cao, D.; Sun, L.; Wang, G.; Lv, Y.; Zhang, M. Kinetics of Hydrogen Peroxide Electroreduction on Pd Nanoparticles in Acidic Medium. *J. Electroanal. Chem.* **2008**, *621*, 31−37.
(61) Li, X.; Heryadi, D.; Gewirth, A. A. Electroreduction Activity of Hydrogen Peroxide on Pt and Au Electrodes. *Langmuir* **2005**, *21*, 9251−9259.
(62) Horányi, G.; Inzelt, G. Study of the Adsorption of Chloride Ions on Platinum Electrodes from Concentrated Solutions of H_2SO_4, H_3PO_4 and $HClO_4$. *J. Electroanal. Chem. Interfacial Electrochem.* **1978**, *86*, 215−218.
(63) Rosso, M.; Giesbers, M.; Arafat, A.; Schroën, K.; Zuilhof, H. Covalently Attached Organic Monolayers on SiC and Si_xN_4 Surfaces:

DOI: 10.1021/acsami.6b05739
ACS Appl. Mater. Interfaces 2016, 8, 18891−18903

Formation Using UV Light at Room Temperature. *Langmuir* **2009**, *25*, 2172−2180.
(64) Lu, K.; Erb, D.; Liu, M. Thermal Stability and Electrical Conductivity of Carbon-Enriched Silicon Oxycarbide. *J. Mater. Chem. C* **2016**, *4*, 1829−1837.
(65) Zhao, H.; Sun, C.; Jin, Z.; Wang, D.-W.; Yan, X.; Chen, Z.; Zhu, G.; Yao, X. Carbon for the Oxygen Reduction Reaction: a Defect Mechanism. *J. Mater. Chem. A* **2015**, *3*, 11736−11739.
(66) Gong, K.; Du, F.; Xia, Z.; Durstock, M.; Dai, L. Nitrogen-Doped Carbon Nanotube Arrays with High Electrocatalytic Activity for Oxygen Reduction. *Science* **2009**, *323*, 760−764.
(67) Bach, R. D.; Dmitrenko, O. The "Somersault" Mechanism for the P-450 Hydroxylation of Hydrocarbons. The Intervention of Transient Inverted Metastable Hydroperoxides. *J. Am. Chem. Soc.* **2006**, *128*, 1474−1488.
(68) Cheng, K.; Yang, F.; Wang, G.; Yin, J.; Cao, D. Facile Synthesis of Porous $(Co,Mn)_3O_4$ Nanowires Free-Standing on a Ni Foam and Their Catalytic Performance for H_2O_2 Electroreduction. *J. Mater. Chem. A* **2013**, *1*, 1669−1676.

DOI: 10.1021/acsami.6b05739
ACS Appl. Mater. Interfaces 2016, 8, 18891−18903